Astronomy & Astrophysics manuscript no. nemgoletter December 2, 2005
(DOI: will be inserted by hand later)

Explosions of O-Ne-Mg cores, the Crab supernova, and subluminous Type II-P supernovae

F.S. Kitaura, H.-Th. Janka, W. Hillebrandt

Max-Planck-Institut für Astrophysik, Karl-Schwarzschild-Str. 1, D-85741 Garching, Germany

December 2, 2005

Abstract. We present results of simulations of stellar collapse and explosions in spherical symmetry for progenitor stars in the 8–10 $M_\odot$ range with an O-Ne-Mg core. The simulations were continued until nearly one second after core bounce and were performed with the PROMETHEUS/VERTEX code with a variable Eddington factor solver for the neutrino transport, including a state-of-the-art treatment of neutrino-matter interactions. Particular effort was made to implement nuclear burning and electron capture rates with sufficient accuracy to ensure a smooth continuation, without transients, from the progenitor evolution to core collapse. Using two different nuclear equations of state (EoSs), a soft version of the Lattimer & Swesty EoS and the significantly stiffer Wolff & Hillebrandt EoS, we found no prompt explosions, but instead delayed explosions, powered by neutrino heating and the neutrino-driven baryonic wind which sets in about 200 ms after bounce. The models eject little nickel ($< 0.015 M_\odot$), explode with an energy of $\gtrsim 0.1 \times 10^{51}$ erg, and leave behind neutron stars (NSs) with a baryonic mass near 1.36 $M_\odot$. Different from previous models of such explosions, the ejecta during the first second have a proton-to-baryon ratio of $Y_e \gtrsim 0.46$, which suggests a chemical composition that is not in conflict with galactic abundances. No low-entropy matter with $Y_e \ll 0.5$ is ejected. This excludes such explosions as sites of a low-entropy r-process. The low explosion energy and nucleosynthetic implications are compatible with the observed properties of the Crab supernova, and the small nickel mass supports the possibility that our models explain some subluminous Type II-P supernovae.

Key words. supernovae: general – neutrinos – hydrodynamics – radiative transfer – nuclear reactions, nucleosynthesis, abundances

1. Introduction

Recent observations of subluminous Type II-P supernovae (SNe) like 2005cs, 2003gd, 1999br and 1997D, have renewed attention to stars near the lower end of the mass range of core-collapse SN progenitors, i.e. to stars with about 8–10 $M_\odot$, which develop O-Ne-Mg cores. A link between both has been suggested because of the low ^{56}Ni ejecta mass and low progenitor luminosities (Chugai & Utrobin 2000, Hendry et al. 2005). However, due to many uncertainties this connection is far from being clear (e.g., Pastorello et al. 2004, 2005; Hamuy 2003; Zampieri et al. 2003, and refs. therein). Also the Crab Nebula's progenitor was proposed to be in this mass window (Gott et al. 1970, Arnett 1975, Woosley et al. 1980, Hillebrandt 1982). The observed composition of the Crab remnant (small C and O abundances, He overabundance) was interpreted as a strong indication that the Crab Nebula comes from a collapsing and exploding progenitor with an O-Ne-Mg core (Davidson et al. 1982, Nomoto et al. 1982, Nomoto 1983).

Moreover, these stars were considered as possible sites for a low entropy r-process (for example, Hillebrandt 1978, Wheeler et al. 1997, Sumiyoshi et al. 2001, Wanajo et al. 2003) based on the assumption that they explode by the prompt bounce-shock mechanism, which Hillebrandt et al. (1984) found to work in a numerical simulation, taking Nomoto's O-Ne-Mg core model (Nomoto 1984, 1987). Such explosions are characterised by the direct propagation of the shock out of the core, the formation of a mass cut, and the continuous acceleration of the material outside of the mass cut to high velocities. They are expected to eject relatively large amounts of neutron-rich matter with low Y_e (~0.2) and low entropies (~ $10 k_B$ per nucleon). However, several groups could not confirm the viability of the prompt explosion mechanism (Burrows & Lattimer 1985, Baron et al. 1987, Mayle & Wilson 1988). Mayle & Wilson (1988) continued their simulations in the post-bounce phase for a longer time and obtained instead a so-called neutrino-driven, delayed explosion (Bethe & Wilson 1985) with a low production of ^{56}Ni (approximately 0.002 $M_\odot$) in agreement with subluminous Type II-P SNe as mentioned above, but with a vast overproduction of neutron-rich material (at least 0.02 $M_\odot$ of ejecta with $Y_e \lesssim 0.41$). The latter finding is inconsistent with the chemical composition of our galaxy, which allows for no more than 10^{-3} $M_\odot$ of material with $Y_e < 0.42$ being ejected per SN (Hartmann et al. 1985). Moreover, the explosion energies of both studies, around 2×10^{51} erg in Hillebrandt et al.'s (1984) model and between 0.6 and 1.2 $\times 10^{51}$ erg in Mayle & Wilson's (1988) simu-

Send offprint requests to: H.-Th. Janka, e-mail: thj@mpa-garching.mpg.de

lations, would be inconsistent with the long plateau phase of the above mentioned subluminous SNe, if their H-envelope masses were $\lesssim 8 M_{\odot}$.

It was suggested that the reason for the discrepant results in the SN simulations of O-Ne-Mg cores (prompt explosions, delayed explosions, no explosions) could be explained by the different nuclear EoSs used by the groups (Fryer et al. 1999). Having in mind that the different approximations in the neutrino transport in previous calculations introduced additional uncertainties, we revisit this topic with a state-of-the-art neutrino transport treatment together with a careful description of weak interactions and including relevant nuclear burning reactions. We additionally make a comparison of collapse and post-bounce calculations with different nuclear EoSs.

2. Numerical techniques and input physics

The transport of neutrinos and antineutrinos of all flavors is done with the energy-dependent solver for the coupled set of moments equations and Boltzmann equation called Vertex. It is described in detail in Rampp & Janka (2002). The equations of hydrodynamics are integrated with the Newtonian finite-volume code Prometheus, which uses a third-order, time-explicit Godunov scheme. This code is a direct implementation of the Piecewise Parabolic Method (PPM), based on a Riemann solver. General relativistic gravity is taken into account approximately by an "effective relativistic potential" according to Marek et al. (2005). Gravitational redshift and time dilation effects are included in the neutrino transport (see Rampp & Janka 2002).

The code is augmented with improved microphysics as described in Buras et al. (2005). It includes also the improved treatment of electron captures on a large variety of nuclei in nuclear statistical equilibrium (NSE), based on shell model Monte Carlo calculations, as described by Langanke et al. (2003). In addition, electron captures on certain important nuclei in the non-NSE regime, in particular ^{20}Ne and ^{24}Mg, are implemented according to Takahara et al. (1989). A simplified treatment of nuclear burning accounts for the main reactions of seven symmetric nuclei (He, C, O, Ne, Mg, Si, Ni). Details about the implemented microphysics will be described in a forthcoming paper (Kitaura et al., in preparation). The nuclear burning reactions considered by Hillebrandt et al. (1984) (^{12}C+^{12}C, ^{16}O+^{16}O, ^{12}C+^{16}O) are all included, taking into account different reaction channels.

To describe matter in NSE, we use two different nuclear EoSs in separate simulations, the Wolff & Hillebrandt (W&H) EoS (Hillebrandt et al. 1984), which is based on Hartree Fock calculations, and the Lattimer & Swesty (L&S) EoS (1991), which is a finite-temperature compressible liquid-drop model and has a compressibility modulus of 180 MeV.

This permits us to compare our models with those of Hillebrandt et al. (1984), in which the Wolff and Hillebrandt EoS was used and which produced prompt explosions. The low-temperature and low-density EoS outside of the NSE regime is described by an ideal gas of nuclei and nucleons, electrons, positrons, and photons (Janka 1999). The switch between NSE and non-NSE description was made in a density- and temperature-dependent manner. The initial model is the same as the one used in previous SN calculations of O-Ne-Mg cores by Hillebrandt et al. (1984) and Mayle & Wilson (1988). It is a 2.2 $M_{\odot}$ He core that corresponds to a progenitor with a main sequence mass of $\sim 8.8 M_{\odot}$ (Nomoto 1984, 1987). Prior to collapse it has an O-Ne-Mg core with $\sim 1.3 M_{\odot}$, surrounded by a C-O shell of about $0.08 M_{\odot}$. We take, however, the initial data at a time when the central density is $\sim 4\times10^{10}$ g/cm^3 and only $\sim$0.1 solar masses at the center of the core have reached nuclear statistical equilibrium (NSE). This is earlier than the starting

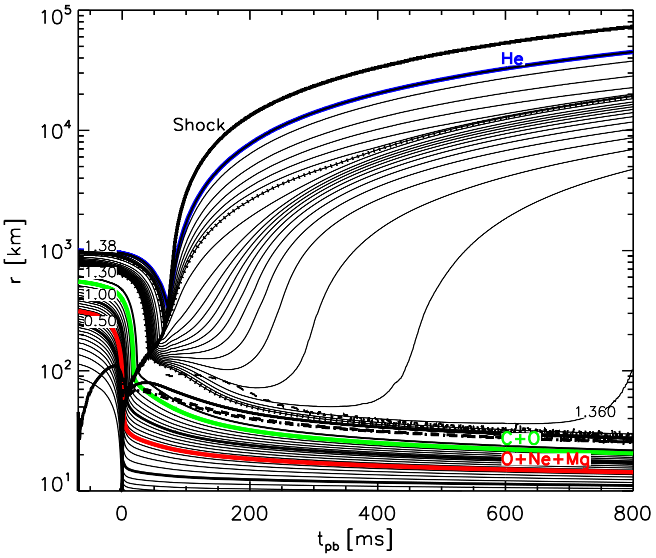

Fig. 1. Mass trajectories for the simulation with the W&H EoS as a function of post-bounce time (t_{pb}). Also plotted: shock position (thick solid line starting at time zero and rising to the upper right corner), gain radius (thin dashed line), and neutrinospheres (ν_e: thick solid; $\bar{\nu}_e$: thick dashed; ν_μ, $\bar{\nu}_\mu$, ν_τ, $\bar{\nu}_\tau$: thick dash-dotted). In addition, the composition interfaces are plotted with different bold, labelled lines: the inner boundaries of the O-Ne-Mg layer at $\sim 0.77\ M_{\odot}$, of the C-O layer at $\sim 1.26\ M_{\odot}$, and of the He layer at $1.3769\ M_{\odot}$. The two dotted lines represent the mass shells where the mass spacing between the plotted trajectories changes. An equidistant spacing of $5\times10^{-2} M_{\odot}$ was chosen up to $1.3579 M_{\odot}$, between that value and $1.3765 M_{\odot}$ it was $1.3\times10^{-3} M_{\odot}$, and $8\times10^{-5} M_{\odot}$ outside.

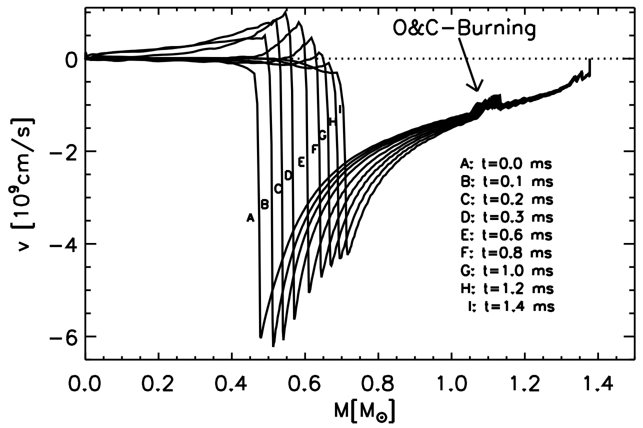

Fig. 2. Velocity profiles vs. enclosed mass at different times for the model with the W&H EoS. Times are normalized to core bounce.

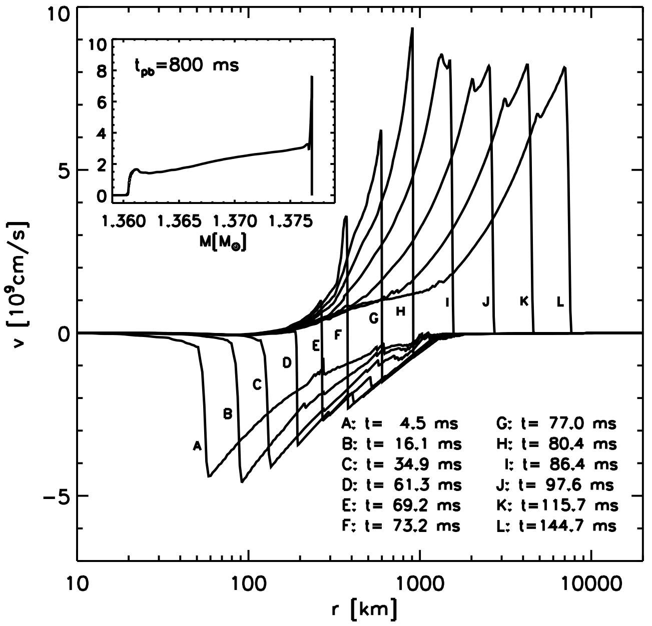

Fig. 3. Velocity profiles as functions of radius for different post-bounce times for the simulation with the W&H EoS. The insert shows the velocity profile vs. enclosed mass at the end of our simulation.

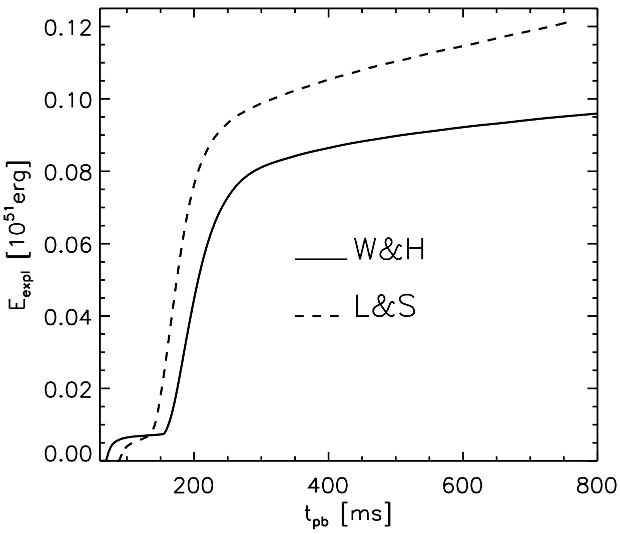

Fig. 4. Explosion energies as functions of time for the simulations with the W&H and L&S EoSs. The energy is defined as the volume integral of the total gas energy (internal plus kinetic plus gravitational) in regions where the latter is positive.

configuration taken by other groups, where the core had already a central density of $\sim 3\times10^{11}$ g/cm^3 and where around 0.3 solar masses were in NSE. Our earlier initial model allows us to trace the evolution of the core towards collapse.

We added a helium atmosphere of about $10^{-4} M_\odot$ around the O-Ne-Mg and C-O core, so that we could move the outer boundary of our Eulerian grid from the core radius of about 1100 km to 100 000 km. For the He-shell profile we adopted a power-law like behaviour of the temperature ($T \propto r^{-1}$) from a 10.2 $M_\odot$ progenitor of A. Heger (private communication), and

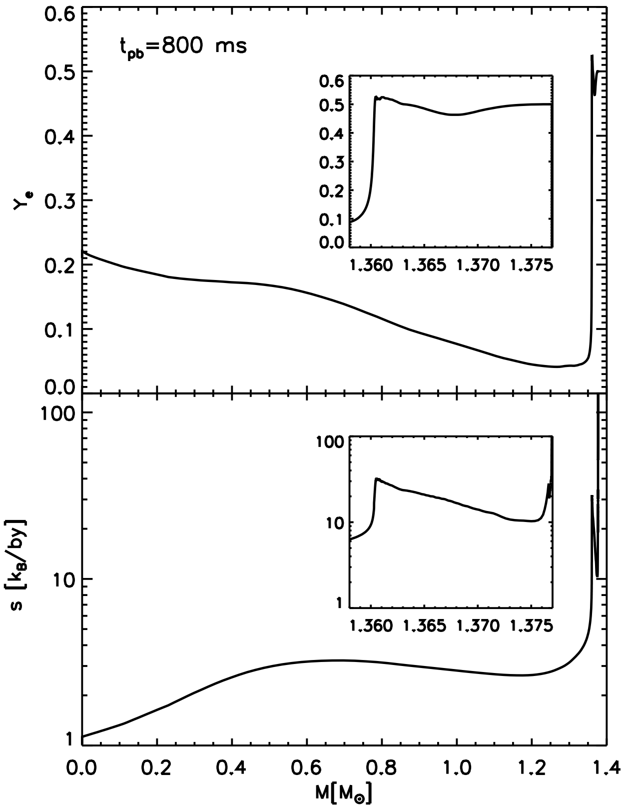

Fig. 5. Profiles of the electron fraction Y_e and entropy s as functions of enclosed mass at the end of our simulation with the W&H EoS.

constructed the density profile by assuming hydrostatic equilibrium, a mass fraction of 100% He, and using the EoS for the low-density regime. We employ in our simulations a very fine mesh in order to resolve the steep density gradient at the outer boundary of the C-O layer, with 1600 nonequidistant zones for the hydrodynamics part. The neutrino transport is done with 235 nonequidistant radial zones.

3. Results

Our results show a very smooth transition from the preceding progenitor evolution to core-collapse. Since O-Ne-Mg cores are gravitationally less bound than more massive stellar progenitors and can release more energy due to nuclear burning, a temperature- and density-dependent treatment of all relevant nuclear burning reactions had to be included, combined with a detailed description of the important electron capture rates. Only that ensured that the progenitor evolution continued towards gravitational collapse without numerical transients. We could therefore confirm that the neutrinos produced by electron captures carry away efficiently the energy that is released by nuclear burning (Miyaji et al. 1980, Miyaji & Nomoto 1987, Hashimoto & Nomoto 1993). A cruder burning treatment, or omission of the improved electron capture rates on nuclei, can have the consequence that the core expands instead of collapsing to a NS, as we verified in test calculations. Fig. 1 shows how the mass shells in the inner region during the first milliseconds start contracting towards the center. The collapse of the core proceeds to higher central densities and when the density of nuclear matter is reached, the EoS "stiffens", and the inner homologous core bounces. The supersonically falling outer layers collide with this central core and a hydrodynamic shock is formed as can be seen in Fig. 1, where this discontinuity in the fluid flow becomes visible by sharp kinks of the mass shell trajectories. This happens after 59 ms of collapse for the calculation with the W&H EoS and after 78 ms in the calculation with the softer L&S EoS. The shock formation radius is at $1.40{\times}10^6$ cm, corresponding to an enclosed mass of $0.475 M_\odot$ in the former case, and at $1.15{\times}10^6$ cm with an enclosed mass of $0.425 M_\odot$ in the second model. This so-called prompt bounce shock produces initially positive velocities in the postshock matter. However, the energy of the shock is insufficient to cause a prompt explosion, and the photodisintegration of nuclei consumes such amounts of energy that the shock is quickly damped and that within only ~1.2 ms after shock formation the velocities are negative everywhere (see Fig. 2 for the case of the W&H EoS). Therefore, the prompt shock mechanism fails, independent of the employed nuclear EoS.

The subsequent expansion of the shock is supported by a combination of different effects. Initially very high mass accretion rates cause the material to pile up between neutrinosphere and shock as it is also observed in the early post-bounce accretion phase of more massive progenitor stars (see, for example, Buras et al. 2005). Second, the rapid decrease of the mass accretion rate contributes to ensure ongoing expansion, because even for quasi-stationary conditions the accretion shock adjusts to a larger radius for smaller mass accretion rates. Finally, as soon as the shock reaches the outer edge of the C-O shell, a very steep density decline leads to an outward acceleration of the shock. The last two aspects are linked to the specific structure of O-Ne-Mg cores and discriminate SN progenitors with such cores from more massive stars. However, despite the shock expansion the material behind the shock has initially still negative velocities and is accreted onto the forming NS (Figs. 1,3). Note that when the matter right behind the shock starts to expand with the shock, the gas accreted by the shock is gravitationally bound and remains so in passing through the shock. However, $p\mathrm{d}V$ work excerted from below and to a minor extent energy input by neutrino heating can convert the accretion into an explosion, accelerating a tiny amount of matter ($\ll 10^{-3}\,M_\odot$) to move outward with the shock.

While the shock reaches larger radii, the temperature and density behind the shock decrease. High-energy electron neutrinos and antineutrinos, which stream off from their neutrinospheres (represented by the thick solid, dashed, and dash-dotted lines in Fig. 1) begin to deposit energy behind the shock mainly by absorption on nucleons, and lead to the formation of a "gain radius" (thin dashed line in Fig. 1) which separates a layer of neutrino cooling around the neutrinosphere from the energy "gain layer" behind the shock (Bethe & Wilson 1985).

About 80 ms after bounce for the L&S EoS and about 60 ms for the W&H EoS, the neutrino heating timescale, defined by the total energy in the gain layer divided by the neutrino heating rate in that region, gets smaller than the advection timescale. The latter is given as the time the accreted matter needs for being advected from the shock to the gain radius. Since the increasing shock radius leads to smaller and smaller postshock velocities, the duration of the deposition of energy via neutrino absorption in the shocked matter increases. The continuous input of energy raises the total energy of the gain layer to a value near zero within roughly 100 ms, unbinding the matter in the gravitational field of the forming NS. The fluid velocity in the layer close to the gain radius therefore starts to become positive (see Figs. 1,3) and the explosion energy shows a rapid increase (Fig. 4).

The cooling region then becomes more and more narrow as the gain radius retreats towards the neutrinosphere, so that neutrinos diffusing out of the contracting protoneutron star begin to heat the layers right above the neutrinosphere. Gas is thus ablated from the NS surface, and the so-called neutrino-driven wind phase sets in at $t \gtrsim 200$ ms after bounce. Several of the mass shells depicted in Fig. 1 clearly show this process.

At this time the energy in the expanding postshock matter has increased to about 0.1×10^{51} erg, rising further due to the power input by the neutrino-driven wind. We extrapolate that the final energy of the explosion will be slightly larger than 0.1×10^{51} erg for the calculation with the W&H EoS and might be about 50% higher in case of the L&S EoS. This is roughly a factor of 10 lower than the canonical SN value, in contrast to the findings in previous explosion models of O-Ne-Mg cores (Hillebrandt et al. 1984, Mayle & Wilson 1988).

At the end of our simulation the mass cut, and therefore the baryon mass of the protoneutron star, is around 1.360 $M_\odot$ for the W&S EoS (Fig. 1) and about 1.363 $M_\odot$ for the L&S EoS. The NS mass will only slightly decrease further because of the ongoing mass loss in the neutrino-driven wind. The mass of the ejecta lies therefore between 0.014 and 0.017 $M_\odot$. The ejected gas has an electron fraction, Y_e, between 0.46 and 0.53 and entropy values between 10 and 40 k_B per nucleon for both EoSs (see Fig. 5 for the case with the W&H EoS). Since only about one third of the ejected matter has a Y_e value very close to 0.5, the mass of ejected ^{56}Ni is certainly smaller than $\sim 0.015 M_\odot$. The Y_e values in our models are higher than those in previous simulations of SNe from O-Ne-Mg cores (Mayle & Wilson 1988). This points to important differences in the neutrino treatment. Spectral Boltzmann transport calculations have recently found early ejecta with $Y_\mathrm{e} \sim 0.5$ and with $Y_\mathrm{e} > 0.5$ also in (artificial) explosions of more massive progenitors (Buras et al. 2005, Fröhlich et al. 2005). The reason for this difference compared to the older models is a refined description of neutrino spectra formation and in particular of charged-current neutrino-nucleon interactions, including the weak magnetism corrections that were pointed out to be relevant by Horowitz (2002).

4. Conclusions

Our 1D simulations of SN explosions from the collapse of O-Ne-Mg cores suggest that such SNe are powered by neutrino heating and by the neutrino-driven wind of the newly formed NS, similar to what Woosley & Baron (1992) found in case of the accretion-induced collapse of white dwarfs to NSs. Such events have a low explosion energy ($\sim 0.1{\times}10^{51}$ erg) and produce little ^{56}Ni ($\lesssim 10^{-2}\,M_\odot$). Most of the ejecta expand initially with velocities of 2–4$\times 10^4$ km s^{-1}, a small fraction has nearly 10^5 km s^{-1}. This is significantly faster than in SNe of more massive progenitors. Of course, sweeping up the matter of the stellar mantle and envelope, the shock will decelerate, and the ejecta velocities after shock breakout from the stellar surface will be correspondingly lower. During the first second of the explosion, the ejected matter has $0.46 \lesssim Y_\mathrm{e} \lesssim 0.53$ and modest entropies ($10 \lesssim s/(k_\mathrm{B}/\mathrm{by}) \lesssim 40$). Such conditions exclude that r-process elements are formed in this matter during this early phase of the explosion of O-Ne-Mg cores: Y_e is too large for the "classical" low-entropy r-process and s is too low for high-entropy r-processing. The ejecta in our models, however, do not show the vast overproduction of some very neutron-rich, rare isotopes like ^{87}Kr, which was made in low-Y_e material ($Y_\mathrm{e} \lesssim 0.44$) in previous simulations (Mayle & Wilson 1988), and which was interpreted as a severe constraint to the rate of such events. Our models yield considerably less energetic explosions than previous simulations and show other significant differences in the dynamics and explosion characteristics. These are probably mainly linked to the improved treatment of neutrino transport and neutrino-matter interactions. While our simulations are spherically symmetric, we do not expect any qualitative changes in the multi-dimensional case, and probably only a modest increase of the explosion energy. Corresponding 2D simulations are in progress.

The small explosion energy obtained in our simulations is more consistent than previous explosion models of O-Ne-Mg cores with the low present expansion velocities (~ 1500 km s^{-1}) of the filaments of the Crab remnant of SN 1054 (Davidson & Fesen 1985), corresponding to a low kinetic energy of 0.6–1.5$\times 10^{50}$ erg for an ejecta mass of $4.6 \pm 1.8\,M_\odot$ in ionized and neutral gas (Fesen et al. 1997). The energy could be even somewhat larger if there were several solar masses of material in an undetected, extended halo.

Based on our findings one might speculate that (B-) stars around $9\,M_\odot$ are also the progenitors of some of the subluminous Type II-P supernovae mentioned in the introduction. In fact, their peculiarities would be explained in a very natural way. The low peak luminosity and extended plateau phase could result from the combination of a low hydrogen envelope mass ($\simeq 6\,M_\odot$) with low expansion velocities ($\lesssim$3000 km/s). The small mass of radioactive ^{56}Ni would explain the low tail-luminosity of these objects. An alternative interpretation of subluminous Type II-P supernovae is the explosion of rather massive stars with extended envelopes, but otherwise more "normal" explosion energies. This connection is supported by the long duration of the plateau phase of many of these events (cf. Pastorello et al. 2004, and refs. therein). Provided the observations cover the full duration of the plateau phase, SN 1997D and 2003gd may still be viable cases for explosions of stars with main sequence masses around 9 $M_\odot$ (Hendry et al. 2005). There is a clear difference between such stars and more massive supernova progenitors. The former eject very little amounts (some $10^{-3}\,M_\odot$?) of oxygen only (Chugai & Utrobin 2000), whereas the latter produce up to a solar mass or more. Therefore one might be able to distinguish between the two scenarios on the basis of observations by measuring the oxygen lines in the late nebular spectra.

Acknowledgements. We are grateful to K. Nomoto for providing us with the initial data and for encouraging discussions. We thank R. Buras and M. Rampp for their input to this work, A. Marek especially for the W&H nuclear EoS, and A. Pastorello, D. Sauer and V. Utrobin for very helpful discussions about SN observations. This work was supported by the Sonderforschungsbereich 375 "Astroparticle Physics" of the Deutsche Forschungsgemeinschaft and by the International Max Planck Research School (IMPRS). Supercomputer time at the Rechenzentrum Garching is acknowledged.

References

Arnett, W.D. 1975, ApJ, 195, 727
Baron, E., Cooperstein, J., & Kahana, S. 1987, ApJ, 320, 300
Bethe, H.A. & Wilson, J.R. 1985, ApJ, 295, 14
Buras, R., Rampp, M., Janka, H.-T., & Kifonidis, K. 2005, A&A, in the press, astro-ph/0507135
Burrows, A. & Lattimer, J. 1985, ApJ, 299, L19
Chugai, N.N. & Utrobin, V.P. 2000, A&A, 354, 557
Davidson, K. & Fesen, R.A. 1985, ARAA, 23, 119
Davidson, K. et al. 1982, ApJ, 253, 696
Fesen, R.A., Shull, J.M., & Hull, A.P. 1997, AJ, 113, 354
Fröhlich, C. et al. 2004, ApJ, in the press, astro-ph/0410208
Fryer, C.L., Benz, W., Herant, M., & Colgate, S. 1999, ApJ, 516, 892
Gott, J.R., Gunn, J.E., & Ostriker, J. P. 1970, ApJ, 160, L91
Hamuy, M. 2001, ApJ, 582, 905
Hartmann, D., Woosley, S.E., & El Eid, M.F. 1985, ApJ, 297, 837
Hashimoto, M., Iwamoto, K., & Nomoto, K. 1993, ApJ, 414, L105
Hendry, M.A. et al. 2005, MNRAS, 359, 906
Hillebrandt, W. 1978, Space Science Reviews, 21, 639
Hillebrandt, W. 1982, A&A, 110, L3
Hillebrandt, W., Nomoto, K., & Wolff, R.G. 1984, A&A, 133, 175
Horowitz, C.J. 2002, Phys. Rev. D, 65, 043001
Janka, H.-T. 1999, unpublished
Langanke, K., Martinez-Pinedo, G., Sampaio, J.M., et al. 2003, Phys. Rev. Lett., 90, 241102
Lattimer, J. & Swesty, F. 1991, Nucl. Phys. A, 535, 331
Marek, A., Dimmelmayer, H., Janka, H.-T., Müller, E., & Buras, R. 2005, A&A, in the press, astro-ph/0502161
Mayle, R. & Wilson, J.R. 1988, ApJ, 334, 909
Miyaji, S. & Nomoto, K. 1987, ApJ, 318, 307
Miyaji, S., Nomoto, K., Yokoi, K., & Sugimoto, D. 1980, Astron.Soc.Jap., 32, 303
Nomoto, K. 1983, Int.Astron.U., 101, 139N
Nomoto, K. 1984, ApJ, 277, 791
Nomoto, K. 1987, ApJ, 322, 206
Nomoto, K., Sparks, W. M., Fesen, R.A., et al. 1982, Nature, 299, 803
Pastorello, A. et al. 2004, MNRAS, 347, 74
Pastorello, A. et al. 2005, MNRAS, submitted
Rampp, M. & Janka, H.-T. 2002, A&A, 396, 361
Sumiyoshi, K., Terasawa, M., Mathews, G.J., et al. 2001, ApJ, 562, 880
Takahara, M., Hino, T., Oda, T., et al. 1989, Nucl. Phys. A, 504, 167
Wanajo, S., Tamamura, M., Naoki, I., et al. 2003, ApJ, 593, 968
Wheeler, J.C., Cowan, J.J., & Hillebrandt, W. 1997, ApJ, 493, L101
Woosley, S.E. & Baron, E. 1992, ApJ, 391, 228
Woosley, S.E., Weaver, T.A., & Taam, R. 1980, in Type I Supernovae, ed. J.C. Wheeler (Austin: University of Texas), p. 96
Zampieri, L. et al. 2003, MNRAS, 338, 711